

Chapter 15

Parametric Optimization of TIG Welding Process on Mechanical Properties of 316L Stainless Steel Using RSM



Subhas Chandra Moi, Asish Bandyopadhyay and Pradip Kumar Pal

Nomenclature

A	Welding current (A)
B	Welding speed (cm/min)
C	Gas flow rate (l/min)
AISI	American Iron and Steel Institute
ANOVA	Analysis of variance
DF	Degree of freedom
GFR	Gas flow rate
PE	Percentage elongation
RSM	Response surface methodology
TIG	Tungsten inert gas
UTS	Ultimate tensile strength

15.1 Introduction

Austenitic stainless steel is an important material and very frequently used in industries like automobile, thermal power plant, nuclear power plant, chemical and pharmaceutical industries due to its superior corrosion resistance, high strength, high ductility, formability and weldability. Out of 300 series grade of austenitic stainless steels, AISI 316L is an extra low carbon version of austenitic chromium-nickel stainless steel [1]. It contains molybdenum materials that improve corrosion resistance, strength at elevated temperatures and improve resistance to pitting from chloride ion solutions. The extra low carbon content in 316L austenitic stainless steels minimizes harmful carbide precipitation due to welding. Some equipment of above said industries is manufactured by fabrication (welding).

S. C. Moi (✉) · A. Bandyopadhyay · P. K. Pal
Mechanical Engineering Department, Jadavpur University, Kolkata, India
e-mail: sc_moi1@rediffmail.com

© Springer Nature Switzerland AG 2019
P. Sahoo and J. P. Davim (eds.), *Advances in Materials, Mechanical and Industrial Engineering*, Lecture Notes on Multidisciplinary Industrial Engineering,
https://doi.org/10.1007/978-3-319-96968-8_15

Tungsten inert gas (TIG) welding is frequently used for fabrication of austenitic stainless steel. TIG welding is basically an electric arc welding process which uses non-consumable tungsten electrode, and arc is established between the tip of an electrode and the workpiece. Inert gas (argon, helium, etc.) is used to avoid contamination of the weldment with air. Sometimes a mixture of any two of the gases mentioned above is also used. TIG welding is used in modern industries for high quality.

The mechanical property of TIG weld is significantly influenced by the parameters of weld pool geometry, namely weld bead width, weld bead height and depth of penetration. And the weld pool geometry is characterized by the levels of different parameters which are used during welding. Therefore, the proper choice of the welding input parameters and its levels are very important for obtaining desired optimal weld pool geometry [2]. Welding current, arc voltage, electrode size, arc travel speed, electrode stick out, etc., are the important welding process parameters. Further, the quality of weld in TIG welding may be influenced due to welding position, electrode composition, edge preparation, the type of gas used and its flow rate. There are different optimization techniques that can be used to determine the required output responses through the development of mathematical equations to postulate the relationships between the input parameters and output variables. One of the most widely used statistical methods of optimization is the response surface methodology (RSM), in which the researchers try to approximate the unknown mechanism with an appropriate empirical model [3–5]. Murugan and Parmer [6] established quadratic relationship between the parameters of MIG welding and parameters of weld pool geometry on 316L austenitic stainless steel. Benyounis et al. [7] used both numerical and graphical optimization techniques to optimize the laser welding parameters on medium carbon steel using RSM. Zhao et al. [8] developed a mathematical model that relates the relationship between the process parameters and weld pool dimensions of laser beam welding of thin gauge galvanized steel. Olabi et al. [9] applied response surface methodology to optimize the laser welding process parameters for joining of dissimilar materials. Ahn et al. [10] optimized laser welding process and reported the effect of welding process parameters on microstructure and mechanical property. Ragavendran et al. [11] studied the hybrid laser and TIG welding process on 316LN stainless steel and developed mathematical models to correlate between input variables and output responses. Padmanaban et al. [12] investigated laser beam welding process through experiment in butt join configuration made by AZ31B magnesium alloy and optimized the process to obtain highest tensile strength. Elatharasan et al. [13] used central composite design technique of response surface methodology to develop a mathematical model to estimate the performance characteristics: ultimate tensile strength, yield strength and elongation in friction stir welding of AA 6061-T6 aluminium alloy material. Srivastava and Garg [14] had carried out experimental analysis to study the effects of the welding process parameters on welding of mild steel plates using gas metal arc welding process by using Box–Behnken design of response surface methodology. Lakshminarayanan et al. [15] had conducted comparative analysis among shielded metal arc welding, gas metal arc welding and gas

tungsten arc welding processes to study the tensile and impact properties of the ferritic stainless steel of thickness 4 mm. Researchers had been found from their study was that gas tungsten arc welding technique was found to be advantageous compared to other welding operations for joining ferritic stainless steels, due to the presence of finer grains in fusion zone and heat-affected zone. Kumar et al. [16] experimentally analysed that parameters of weld bead geometry are largely dependent on incident angle for laser welding. They also optimized the welding process for obtaining maximum value of tensile strength by RSM. Ghosh et al. [17] applied grey-based Taguchi method on the experiment of MIG welding on 316L stainless steel. They concluded that the welding current is the most significant factor for obtaining highest joint strength.

From the literature survey, it is found that various aspects of TIG welding like parametric studies, mathematical modelling and process optimization have been explored by the investigators. But work done by them appears not sufficient, as reliable databank has not yet been established and that can be obtained through many more extensive researches involving parametric studies, analysis of the response in terms of quality like joint strength, microstructures particularly in the field of TIG welding of 316L stainless steel. This sound knowledge base and precise understanding will help in controlling the TIG welding process more reliably and predicatively. In practice, one will be able to select proper parametric combination depending upon the level of quality required. This will also help automatic/ intelligent control of the process. Hence, the present work is one attempt towards the improvement of weld joint quality by selection of proper process parameters and to enrich the existing knowledge base in the area of TIG welding.

15.2 Experimental Procedures

In order to achieve desired aim, the research work has been considered in the following sequence:

- (i) Selecting the base metal and filler metal.
- (ii) Identifying the most significant TIG welding parameters and their levels.
- (iii) Selecting the design of experiment and constructing experimental design matrix.
- (iv) Performing the experiments according to design matrix.
- (v) Testing of welded samples through non-destructing and destructive testing methods and recording the responses like UTS, PE.
- (vi) Developing a regression model using RSM and identifying the significant factors.
- (vii) Verifying the predicted results for optimization through confirmatory test.

The base material has been selected as 316L austenitic stainless steel of dimension 50 mm × 80 mm × 3 mm. ER316L austenitic stainless steel of diameter 1.6 mm has been taken as a filler material. The chemical composition of the base material

Table 15.1 Composition of the base material and filler material

Weight %	C	Mn	Si	S	P	Cr	Ni	Mo	Cu	Fe
AISI 316L	0.026	0.97	0.26	0.012	0.043	16.12	10.08	2.03	0.15	70.31
ER 316L	0.040	1.50	0.45	0.03	0.030	18.20	12.00	2.30	0.75	64.70

Table 15.2 Mechanical properties of base material

Ultimate tensile strength (MPa)	Yield strength (MPa)	% elongation	Hardness (VHN)
608.88	306.92	12.02	212

and filler material and its mechanical properties are given in Tables 15.1 and 15.2, respectively.

The most influencing parameters which affect weld pool geometry as well as mechanical properties of TIG welded joint are identified through extensive literature survey and previous work done. The important identified process parameters are welding current, gas flow rate and welding speed. A large number of trials have been performed on 3-mm-thick AISI 316L stainless steel plates to find out the efficient and practicable working limits of TIG welding parameters, and this has been done by altering one of the selected parameters while others remain constant. The visual inspection and non-destructive tests have been used to identify the working limits of the welding process parameters. Table 15.3 shows the identified welding parameters along with their three levels.

The experimental design matrix has been developed according to the Box–Behnken design of response surface methodology (RSM). RSM is a collection of mathematical and statistical techniques used for modelling and optimizing engineering problems where response is influenced by several input variables. In Box–Behnken design of RSM, there should be at least three factor and three levels for each factor. The upper limit of each parameter is coded as ‘+1’, and the lower bound is coded as ‘-1’. The design of experiment software, Minitab v17, has been applied to build up the experimental design matrix for RSM. Table 15.4 represents the experimental plan.

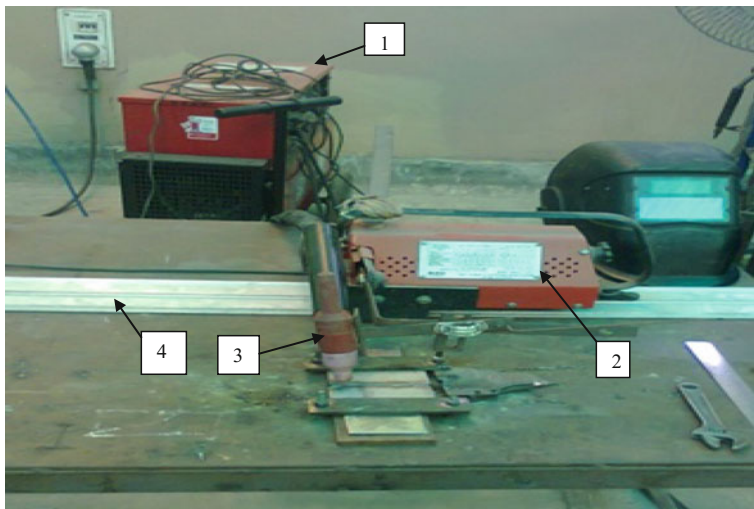
The experiments have been planned and conducted according to a Box–Behnken design of response surface methodology. Figure 15.1 shows the photographic view of a semi-automatic TIG welding machine (Model—SUPERGEN320, M/C SR.

Table 15.3 Process parameters and their levels

Parameters	Units	Notation	Levels		
			-1	0	+1
Welding current	A	A	100	125	150
Travel speed	cm/min	B	12	15	18
Gas flow rate	l/min	C	6	9	12

Table 15.4 Experimental design matrix as per RSM

Exp. no.	Welding current		Travel speed		Gas flow rate	
	Coded	Uncoded (A)	Coded	Uncoded (cm/min)	Coded	Uncoded (l/min)
1	-1	100	-1	12	0	9
2	1	150	-1	12	0	9
3	-1	100	1	18	0	9
4	1	150	1	18	0	9
5	-1	100	0	15	-1	6
6	1	150	0	15	-1	6
7	-1	100	0	15	1	12
8	1	150	0	15	1	12
9	0	125	-1	12	-1	6
10	0	125	1	18	-1	6
11	0	125	-1	12	1	12
12	0	125	1	18	1	12
13	0	125	0	15	0	9
14	0	125	0	15	0	9
15	0	125	0	15	0	9



1-welding machine, 2-travel car, 3-TIG torch, 4- track

Fig. 15.1 Photographic view of experimental set-up

No-12111097670 and Make—Ador Welding Ltd.) Here, the TIG torch has been fixed to the travel car to confirm the torch is set at a predetermined angle. The travel car travels on the defined path and can move only straight line direction. Control of current, speed and gas flow rate is done manually for each run. All plates of size 50 mm × 80 mm × 3 mm and filler rods are cleaned by stainless steel wire brush with acetone for removing the dust, oil, grease and thin oxide coating before welding. Square butt joint configurations have been prepared by tungsten inert gas welding using argon with purity 99.99%, as shielding gas. The welding direction has been taken as normal to the direction of rolling. During welding, the workpieces have been placed on copper plate and mechanical clamps are also used for avoiding distortion.

15.3 Results and Discussions

Square butt welded joints are being made under varied welding input factors, and then quality of weld is being judged, first by visual inspection and then by non-destructive and destructive testing methods. In so far a non-destructive test is concerned, X-ray radiography has been taken up. Tensile test specimens have been prepared, and tensile test has been performed for all the samples.

15.3.1 Visual Inspection

A visual inspection examines the quality of weldment such as bead appearance, width and thickness, welding defects like undercut, cracks, pits and slag inclusions in the surfaces of the welded joints, and whether the throat is as thick as desired, and the misalignment is within the allowable allowance. The visual inspection of welded joints is easy, simple, inexpensive and is capable of inspecting many weld zones at one time. Therefore, it is generally used for any type of welds. Photographic view of two welded specimens, sample number 1 and sample number 14, is shown in Fig. 15.2.

Visual inspection has been carried out for all the welding samples after welding. The observed results are given in Table 15.5. The defects observed in the visual inspection in some of the samples include: little undercut at the end, large reinforcement height, lack of penetration. Under certain parametric conditions, almost no defects are found in a few samples like sample numbers 2, 5, 8, 9, 12, 13, 14 and 15. The possible reasons for the defects found in several samples are due to lack of environmental suitability, fluctuation of voltage and due to semi-automatic machine set-up, etc. Further, the skill of the operator or technician is very crucial for weld quality. Defects may come from any type of irregularities/inhomogeneity in the base metal as well as filler wire. Undercut defect may be caused by inappropriate joint geometry in some of the samples. It may have been resulted because of

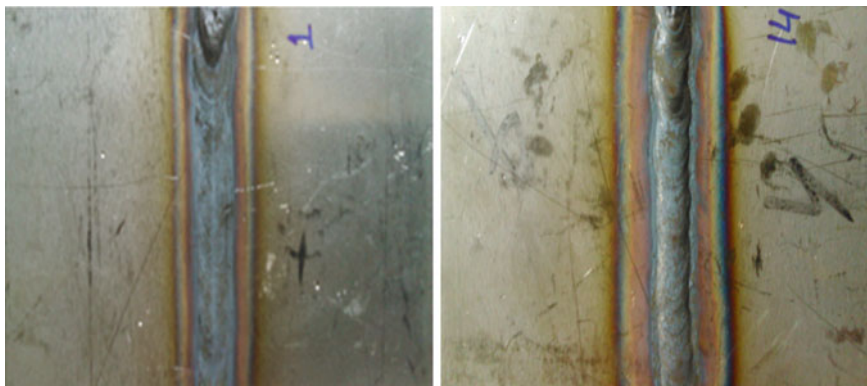


Fig. 15.2 Photographic view of welded sample number 1 and 14

Table 15.5 Results of visual inspection

Exp. no.	Current (A)	Speed (cm/min)	GFR (l/min)	Observations
1	100	12	9	Large reinforcement height at the starting, good penetration
2	150	12	9	Uniform penetration and uniform weld bead
3	100	18	9	Lack of penetration at the end
4	150	18	9	Little undercut at the end
5	100	15	6	Good penetration throughout
6	150	15	6	Large reinforcement height
7	100	15	12	Lack of penetration at the end
8	150	15	12	Uniform HAZ width, no defect
9	125	12	6	Good penetration throughout
10	125	18	6	Minimum porosity but good penetration throughout
11	125	12	12	Lack of penetration at the end
12	125	18	12	Uniform penetration and uniform weld bead
13	125	15	9	Good penetration throughout
14	125	15	9	Uniform penetration and uniform weld bead
15	125	15	9	Good penetration throughout

excessive welding current and voltage. The combined effects of various welding input parameters can also form undercut defect on weldment. Lack of penetration is one of the main defects which will affect the joint strength of the welded sample. The reasons for lack of penetration are faster travel speed, incorrect selection of welding currents levels, improper cleaning of welding zone, and presence of oxides, scale and other impurities which do not allow the deposited metal to fuse accurately with the base metal.

15.3.2 X-Ray Radiography Test

X-ray is used to determine the internal soundness of welds. This examination has been done for all 15 welded joints after the visual inspection by XXQ-2005 X-ray flaw detector. Table 15.6 illustrates the results of X-ray radiography examination. It is noticed that almost all the samples pass through X-ray radiography test with no significant defect remarks. Only sample number 11 is found with defect like lack of penetration. Lack of penetration is most significantly affecting the strength of the weld. Lower heat input, improper choice of current or less skill of the welder, etc., [18] as pointed out earlier, are the major causes for lack of penetration defect. Hence, this sample has been replaced by a new one done by same welding condition.

Qualities of the joints are further evaluated by other tests and studies, as well. If the results of visual inspection and the results of X-ray radiography test are compared, then some consistency can be observed. It is found from the two tables (Tables 15.5 and 15.6) that low current is not the primary cause of lack of penetration, because for sample numbers 1, 3, 5 and 7 also have the current level 100A, but for these samples, no defect is found. The skill of the welding operator is high depending on weld quality. Lack of penetration defect may also come from any irregularities in the base metal or filler wire as mentioned earlier in case of visual inspection. Large electrode angle may also be a possible reason for this type of defect. Any improper welding environment can also affect the weld quality. This may have occurred due to entrapped gas in the weld pool, which could have been

Table 15.6 Results of X-ray radiography test

Exp. no.	Current (A)	Speed (cm/min)	GFR (l/min)	Observations	Remarks
1	100	12	9	No significant defect	Acceptable
2	150	12	9	No significant defect	Acceptable
3	100	18	9	No significant defect	Acceptable
4	150	18	9	No significant defect	Acceptable
5	100	15	6	No significant defect	Acceptable
6	150	15	6	No significant defect	Acceptable
7	100	15	12	Minimum porosity	Acceptable
8	150	15	12	No significant defect	Acceptable
9	125	12	6	No significant defect	Acceptable
10	125	18	6	Minimum porosity	Acceptable
11	125	12	12	Lack of penetration	Not satisfactory
12	125	18	12	No significant defect	Acceptable
13	125	15	9	No significant defect	Acceptable
14	125	15	9	No significant defect	Acceptable
15	125	15	9	No significant defect	Acceptable

avoided by proper selection of gas flow rate and arc gap. A faster travel speed and too small root gap may also be the reasons for such defect. Therefore, defects may possibly appear from inappropriate choice of different welding parameters, namely current, voltage, arc gap, including their ranges also. It is noticed from the tables of visual as well as radiography examination that almost no welding defects are observed, when welding with middle value of current, speed and gas flow rate. It is also found from visual inspection and X-ray radiographic examination that no significant defect presences in sample numbers 2, 5, 9 and 12. Thus, this is the reason for obtaining higher value tensile properties of the samples under tensile testing.

15.3.3 Tensile Test

After X-ray radiography test, tensile test samples have been prepared in accordance with ASTM E8 M-04. Tensile specimens of the weld joint are obtained in taking specimen from transverse direction of weld joint. Top view of weldment in butt joint configuration is shown in Fig. 15.3. Figure 15.4 represents typical diagram showing the dimensions of the standard sub-size tensile specimen. Tensile test of all welded samples has been conducted in universal testing machine (Model—8801, Make—INSTRON and capacity—100 kN) at strain rate of 0.001/s. The tensile properties mainly UTS, yield strength, percentage elongation, of base metal as well as TIG welded joints have been evaluated. The measured responses (UTS and PE) are listed in Table 15.7.



Fig. 15.3 Top view of welded sample in butt joint configuration

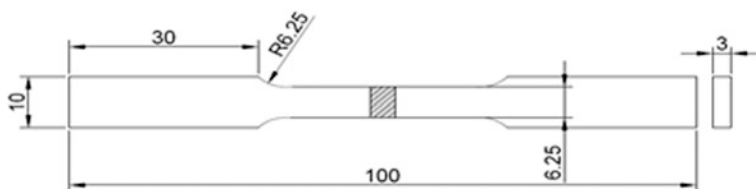


Fig. 15.4 Schematic diagram of TIG welded sample for tensile test

Table 15.7 Design matrix and experimental results

Run	Current (A)	Speed (cm/min)	GFR (l/min)	UTS (MPa)	% elongation
1	100	12	9	612.36	08.53
2	150	12	9	616.68	11.94
3	100	18	9	609.94	10.24
4	150	18	9	630.55	11.05
5	100	15	6	621.46	10.45
6	150	15	6	612.89	13.47
7	100	15	12	580.61	11.45
8	150	15	12	607.75	13.18
9	125	12	6	624.09	10.16
10	125	18	6	616.98	09.60
11	125	12	12	592.44	10.12
12	125	18	12	615.92	11.56
13	125	15	9	639.84	14.68
14	125	15	9	645.31	14.44
15	125	15	9	642.46	14.58

15.3.4 Developing the Mathematical Models: Regression Analysis

In the present study, Minitab v17 software has been applied to the experimental data to obtain the quadratic mathematical equations for ultimate tensile strength (UTS) and percentage elongation (PE). This regression equations/ mathematical model is used for predicting responses (UTS and PE) in terms of current, speed and gas flow rate. It consists of the effect of main parameters and first-order interaction of all parameters.

15.3.4.1 Ultimate Tensile Strength (UTS)

In the present context, the response i.e. ultimate tensile strength (σ) is function of TIG welding current (A), travel speed (B) and gas flow rate (C) and it can be expressed as

$$\sigma = f(\text{welding current, travel speed, gas flow rate})$$

$$\sigma = f(A, B, C) \quad (15.1)$$

Typically, a second-order polynomial equation is used in RSM that is provided below:

$$Y = b_0 + \sum_{i=1}^k (b_i x_i) + \sum_{i=1}^k (b_{ii} x_i^2) + \sum \sum (b_{ij} x_i x_j) + \epsilon \quad (15.2)$$

where

- Y response variables, i.e. dependent variables
- x_i predicted variables, i.e. independent variables
- b_0 model constant
- ϵ random error.

Parameters b_i , b_{ii} , b_{ij} are known as regression coefficient, where $i = 1, 2, 3, \dots k$ and $j = 1, 2, 3, \dots k$.

In the study, three parameters have been considered. Therefore, for three factors, the selected polynomial equations can be provided as:

$$\sigma = b_0 + b_1(A) + b_2(B) + b_3(C) + b_{11}A^2 + b_{22}B^2 + b_{33}C^2 + b_{12}(AB) + b_{13}(AC) + b_{23}(BC) \quad (15.3)$$

where σ is the predicted response, b_0 model constant, b_1 , b_2 and b_3 linear coefficients, b_{11} , b_{22} and b_{33} quadratic coefficients and b_{12} , b_{13} and b_{23} cross-interaction coefficients.

The second-order regression equation for the response UTS in terms of coded factors is given below:

$$\begin{aligned} \text{UTS} = & 160.6 + 4.699 A + 17.51 B + 10.98 C - 0.02547 A * A - 1.026 B * B - 2.327 C * C \\ & + 0.0543 A * B + 0.1190 A * C + 0.850 B * C \end{aligned} \quad (15.4)$$

The adequacy of the developed model for UTS has been tested using the statistical analysis of variance (ANOVA) technique. Table 15.8 shows the adequate ANOVA test results for UTS. From table, it is found that the regression is significant with linear and quadratic terms for UTS at 95% confidence level as its p value is less than 0.05. The lack-of-fit value of the model is not significant which is desirable. The model indicates that the welding process parameters: current (A), speed (B) and gas flow rate (C) and its squared terms [current*current (A^2), speed*speed (B^2) and gas flow rate*gas flow rate (C^2)] and interaction effects [current and speed ($A \times B$), current and gas flow rate ($A \times C$) and speed and gas flow rate ($B \times C$)] have significant effect on UTS. The 'R²' value is 0.9895, and 'Pred R²' of 0.8805 is in reasonable agreement with the 'Adj R²' of 0.9707. The 'R²' value is higher and nearer to 1, that is desirable.

The ANOVA result indicates that the gas flow rate is most significantly effects ultimate tensile strength followed by welding current and speed.

Table 15.8 ANOVA results for testing adequacy of the UTS

Source	DF	Adj SS	Adj MS	F-value	P value	
Model	9	4268.93	474.33	52.59	0.000	Significant
Linear	3	1107.49	369.16	40.93	0.001	Significant
A—current	1	236.53	236.53	26.23	0.004	Significant
B—travel speed	1	96.74	96.74	10.73	0.022	Significant
C—gas flow rate	1	774.21	774.21	85.84	0.000	Significant
Square	3	2542.36	847.45	93.96	0.000	Significant
A*A	1	935.46	935.46	103.72	0.000	Significant
B*B	1	315.04	315.04	34.93	0.002	Significant
C*C	1	1619.34	1619.34	179.54	0.000	Significant
Two-way interaction	3	619.08	206.36	22.88	0.002	Significant
A*B	1	66.34	66.34	7.36	0.042	Significant
A*C	1	318.80	318.80	35.35	0.002	Significant
B*C	1	233.94	233.94	25.94	0.004	Significant
Error	5	45.10	9.02			
Lack of fit	3	30.13	10.04	1.34	0.454	Not significant
Pure error	2	14.97	7.48			
Total	14	4314.02				

Model summary

S R² R² (adj) R² (pred)

3.00320 98.95% 97.07% 88.05%

15.3.4.2 Percentage Elongation (PE)

The second-order regression equation for the response, percentage elongation is developed by using RSM, in terms of coded factors is given below:

$$\begin{aligned}
 PE = & -121.13 + 0.6834 A + 10.494 B + 2.323 C - 0.001879 A * A - 0.3280 B * B \\
 & - 0.1394 C * C - 0.00867 A * B - 0.00430 A * C + 0.0556 B * C
 \end{aligned}
 \tag{15.5}$$

Table 15.9 shows the adequate ANOVA test results for percentage elongation (PE), and it is found that model is significant ($P < 0.05$) at 95% confidence level or 5% significant level. The lack-of-fit value of the model is not significant which is desirable. The model F-value is 119.66 which indicates that the model is significant. Here $A, B, C, A^2, B^2, C^2, A \times B, A \times C,$ and $B \times C$ are the significant model terms. The ‘R²’ value is 0.9954, and ‘Pred R²’ of 0.9335 is in reasonable agreement with the ‘Adj R²’ of 0.9871. The ‘R²’ value is higher and nearer to 1, that is desirable.

According to the mathematical models, it is understood that gas flow rate is found to be the most important factor affecting UTS and current is the most significant parameter on percentage elongation. But welding speed is insignificant factor for ultimate tensile strength and percentage elongation.

Table 15.9 ANOVA results for testing adequacy of percentage elongation (PE)

Source	DF	Adj SS	Adj MS	F-value	P value	
Model	9	53.3411	5.9268	119.66	0.000	Significant
Linear	3	11.2835	3.7612	75.94	0.000	Significant
A—current	1	10.0576	10.0576	203.07	0.000	Significant
B—travel speed	1	0.3613	0.3613	7.29	0.043	Significant
C—gas flow rate	1	0.8646	0.8646	17.46	0.009	Significant
Square	3	38.9516	12.9839	262.15	0.000	Significant
A*A	1	5.0941	5.0941	102.85	0.000	Significant
B*B	1	32.1777	32.1777	649.68	0.000	Significant
C*C	1	5.8116	5.8116	117.34	0.000	Significant
Two-way interaction	3	3.1060	1.0353	20.90	0.003	Significant
A*B	1	1.6900	1.6900	34.12	0.002	Significant
A*C	1	0.4160	0.4160	8.40	0.034	Significant
B*C	1	1.0000	1.0000	20.19	0.006	Significant
Error	5	0.2476	0.0495			
Lack of fit	3	0.2186	0.0729	5.01	0.171	Not significant
Pure error	2	0.0291	0.0145			
Total	14	53.5887				

Model summary

S R² R²(adj) R²(pred)

0.222550 99.54% 98.71% 93.35%

The soundness of the developed model has also been checked by the normal probability plot of the residuals for UTS and PE as shown in Figs. 15.5 and 15.6, respectively. From figure, it is seen that the residuals are falling on the straight line, which means the errors are distributed normally and the mathematical relationship is correctly developed.

15.3.5 Effect of TIG Welding Process Parameters on UTS

The surface and contour plots have been drawn from Eq. 15.4 to study the interaction effects of process parameters on UTS and shown in Figs. 15.7, 15.8 and 15.9. It is observed that UTS first increases gradually then decreases with the increase in the levels of the welding process parameters. From Fig. 15.7a, b, it is noticed that UTS increases with gas flow rate (GFR) and then starts decreasing to its minimum value. UTS is maximum at medium values of GFR and welding current. Figure 15.8a, b shows the combined effect of welding speed and welding current on UTS. It is found that UTS is maximum at the medium values of welding speed and current. The interaction between GFR and welding speed on UTS is shown in

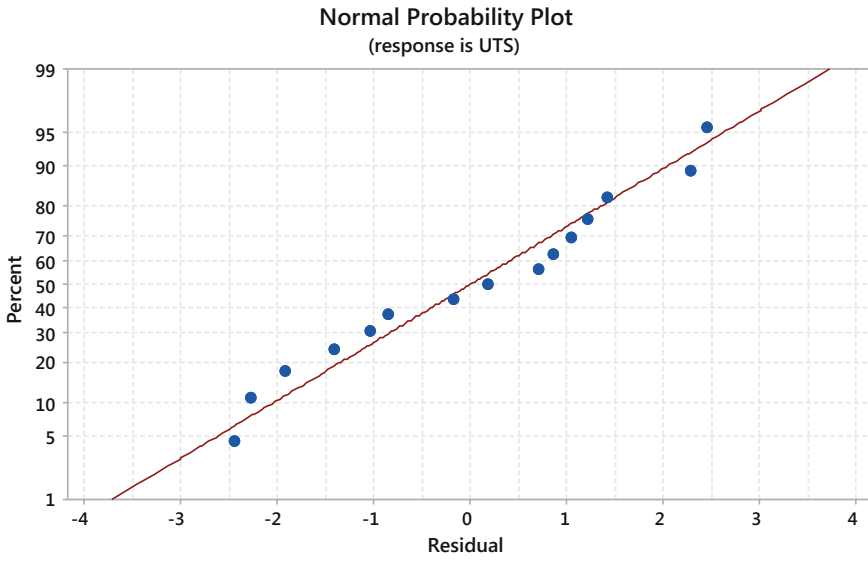


Fig. 15.5 Residual plot of tensile strength

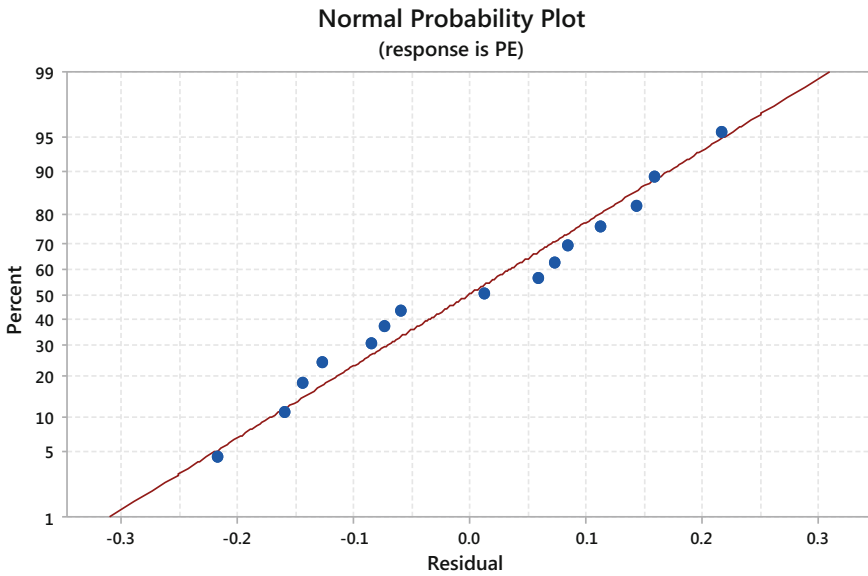


Fig. 15.6 Residual plot of percentage elongation

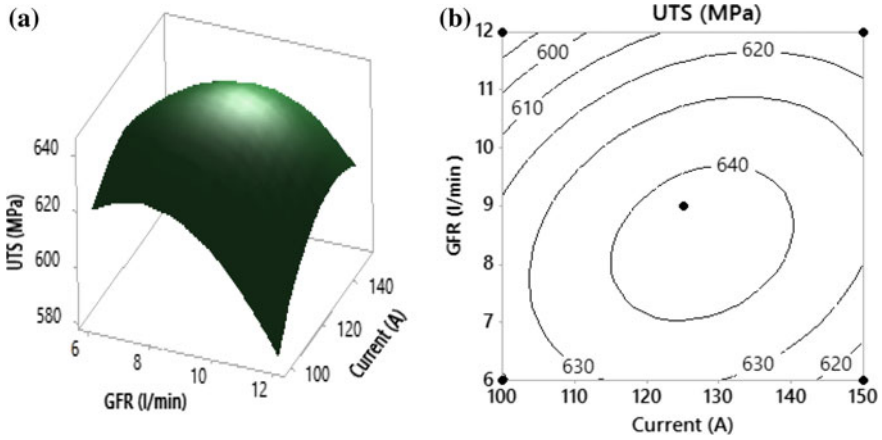


Fig. 15.7 a Response surface plot and b contour plot showing the effect of GFR and current on the UTS at welding speed of 15 cm/min

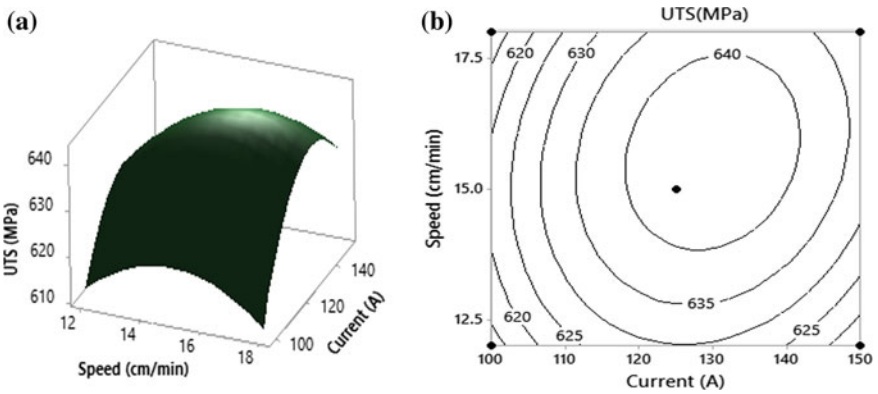


Fig. 15.8 a Response surface plot and b contour plot showing the effect of welding speed and current on the UTS at GFR of 9 l/min

Fig. 15.9a, b. It is observed that the UTS is optimum at the middle value of GFR and welding speed.

The main effect plots for UTS with process parameters like welding current, travel speed and GFR are shown in Fig. 15.10. The graph indicates that UTS increases from low value to maximum value, when current increases from 100 to 130 A as depth of penetration attains its maximum value. Similar types of patterns are also seen in case of welding speed and GFR. As welding speed changes from 12 to 15 cm/min, UTS increases from 630 to 643 MPa. GFR increases from 6 to 9 l/min UTS increases from 628 to 643 MPa due to decrease in porosity level of weld metals.

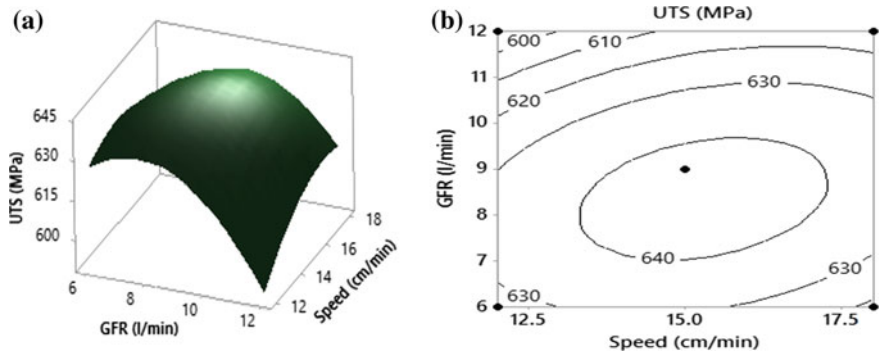


Fig. 15.9 a Response surface plot and b contour plot showing the effect of GFR and speed on the UTS at welding current of 125 A

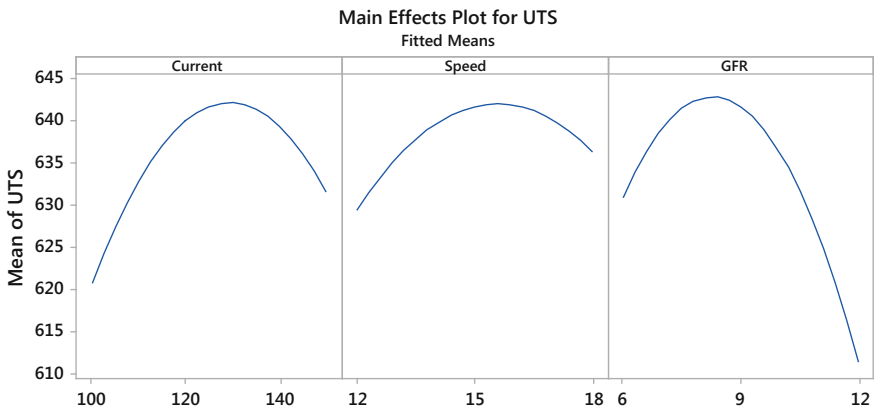


Fig. 15.10 Main effect plot for UTS

15.3.6 Effect of TIG Welding Process Parameters on PE

Figures 15.11, 15.12 and 15.13 illustrate the response surface plot and contour plot for the response of percentage elongation. Similar type of patterns is also observed in case of percentage elongation. The interactive effects of welding speed and GFR on percentage elongation are shown in Fig. 15.11a, b. The value of percentage elongation is maximum at the medium levels of both welding speed and GFR. Cooling rate decreases with increase in heat input at low welding speed. This in turn will take longer time for solidification. As a result, it produces coarse grain, hence low tensile strength and low percentage elongation. The combined effect of GFR and welding current on percentage elongation is shown in Fig. 15.12a, b. Welding current has a significant effect on PE. At lower welding current, the percentage

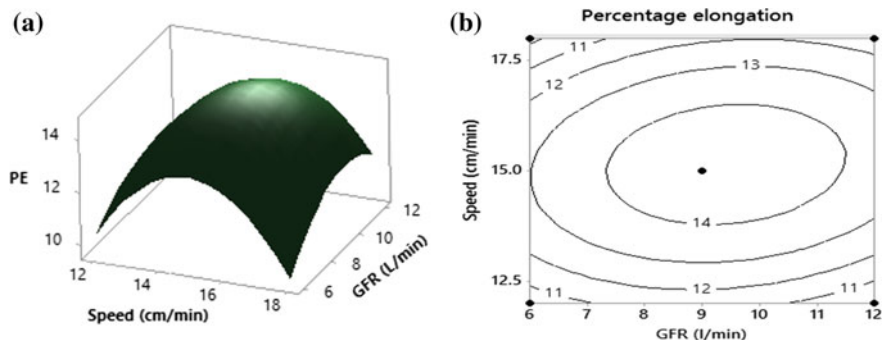


Fig. 15.11 a Response surface plot and b contour plot showing the effect of welding speed and GFR on the PE at current of 125 A

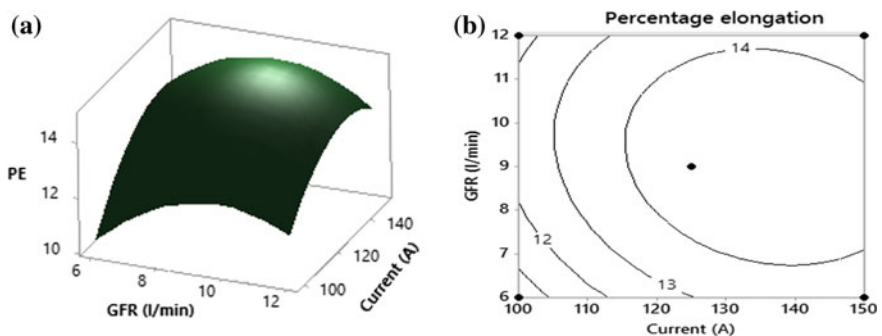


Fig. 15.12 a Response surface plot and b contour plot showing the effect of GFR and current on the PE at welding speed of 15 cm/min

elongation of the welded joint is lower. When current is increased, the PE is also increased and reached its maximum value as it forms uniform penetration. Figure 15.13a, b demonstrates the interaction effect of welding speed and welding current on percentage elongation at GFR of 9 l/min.

Figure 15.14 represents the main effect plot of percentage elongation with welding current, welding speed and GFR. The value of percentage elongation increases as welding current increases from 100 to 130 A due to proper penetration. As travel speed changes from 12 to 15 cm/min, PE achieves its greatest value. For further increase in the level of welding speed, the PE starts to decrease. PE reaches its optimum value when GFR changes from 6 to 9 l/min.

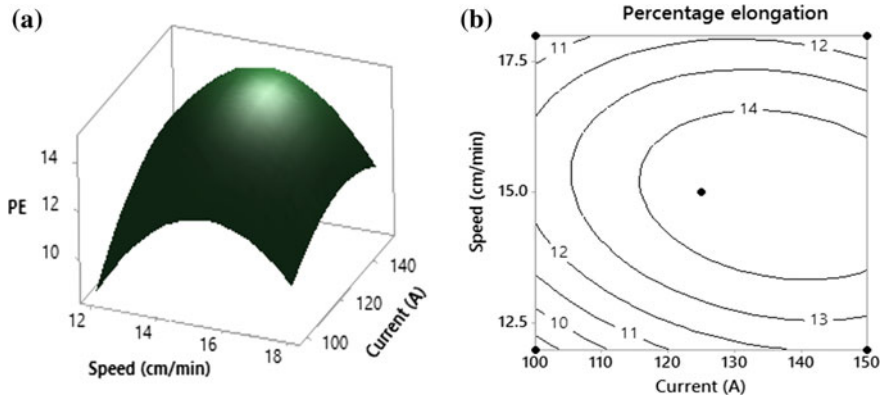


Fig. 15.13 a Response surface plot and b contour plot showing the effect of welding speed and current on the PE at GFR of 9 l/min

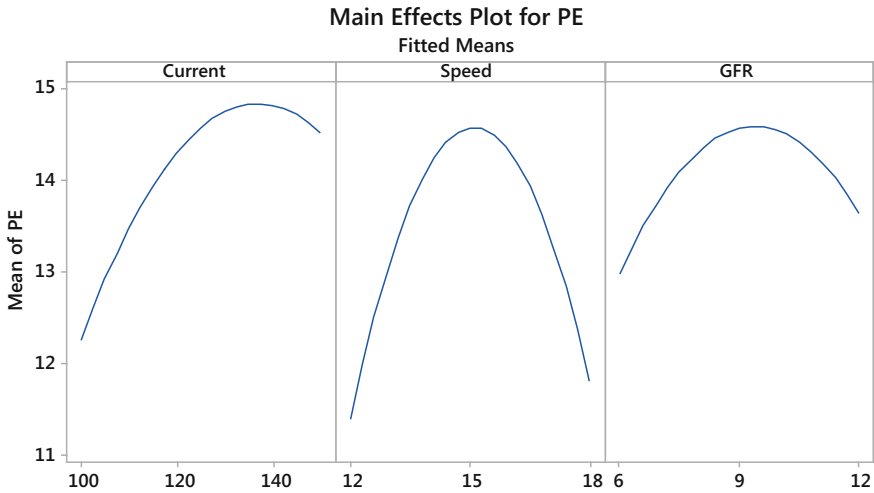


Fig. 15.14 Main effect plot for percentage elongation

15.3.7 Optimization of Ultimate Tensile Strength

One of the main targets of experimental work related to welding is to attain higher tensile strength and as well as percentage elongation. In the study, the aim is to achieve maximum ultimate tensile strength and maximum percentage elongation of welded specimens simultaneously which is desirable for good quality of welded joint. The results optimization done by RSM for UTS and PE is shown in Fig. 15.15. In this figure, each column represents one of the TIG welding process parameters and each row of the graph represents a response like UTS, PE and how

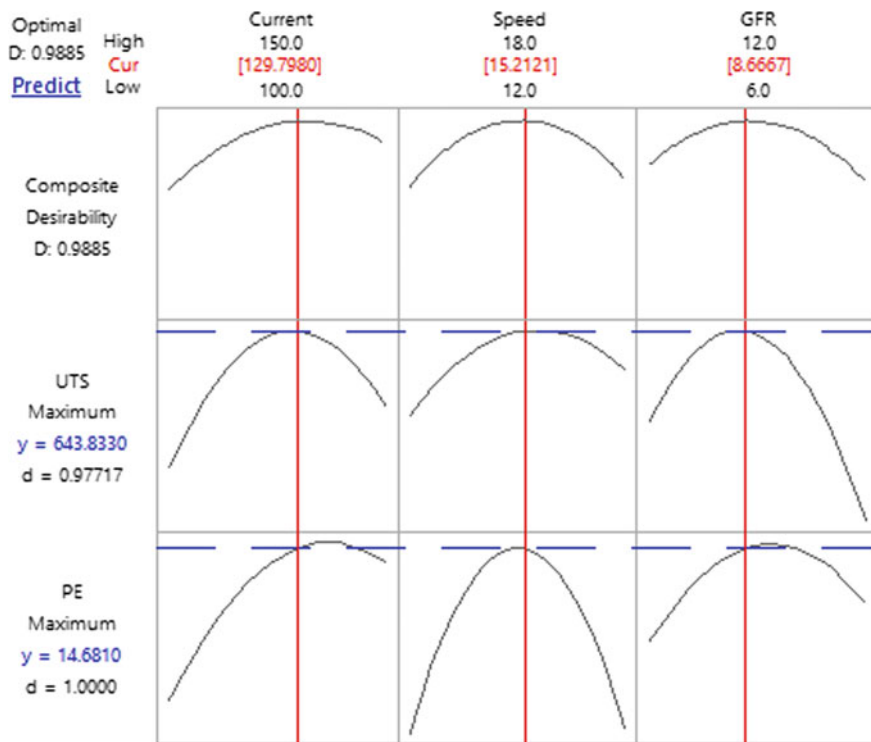


Fig. 15.15 Optimization results of ultimate tensile strength and percentage elongation

this response variable alters as a function of the welding process parameters, while maintaining other process parameters unchanged. The optimum predicted response values are shown by horizontal dotted lines, and corresponding optimum process parameters are designated by vertical line inside the graph. At the top of the column shows the values of optimum process parameters, and left-hand side shows the predicted responses values. Individual desirability values are also given in this figure. The design of experiment software, Minitab v17, has been applied for optimization of TIG welding process. The most favourable ultimate tensile strength, 643.83 MPa, and optimum percentage elongation, 14.68, have been obtained at welding current of 129.8 A, welding speed of 15.2 cm/min and gas flow rate of 8.7 l/min. The value of composite desirability factor, $D = 0.9885$.

Microstructural examination has been carried out by scanning electron microscopy (SEM) of base material and weld material of the welded joint that has been prepared with optimum parametric setting as mentioned earlier. Figure 15.16a, b represents typical SEM micrographs of base and weld metal, respectively. Base material mostly consists of austenitic structure along with little annealing twins. From Fig. 15.16b, it is found that very fine skeletal δ -ferrite is produced in weld

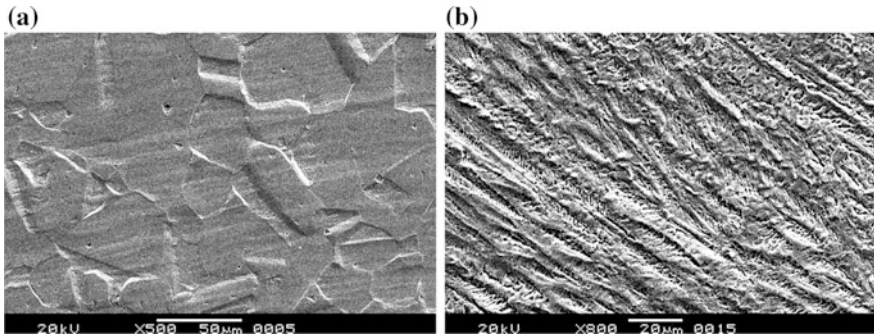


Fig. 15.16 SEM micrographs of **a** base metal and **b** weld zone

Table 15.10 Multi-objective optimization results

Optimum condition					
A (A)	B (cm/min)	C (l/min)		UTS (MPa)	PE
129.8	15.2	8.7	Average actual predicted Error %	650.45	14.75
				643.83	14.68
				1.02	0.47

area and reasonable precipitation. These are the most important causes for obtaining optimum tensile strength and percentage elongation of the said TIG welded joint.

15.4 Confirmation Test

The results of optimization obtained have been validated by performing confirmatory experiments. Table 15.10 represents the results of confirmatory tests that are conducted at optimum conditions. It is noticed from table that the error in terms of percentage between the predicted and experimental results is very small. This indicates that the optimized TIG welding process parameters can be considered to obtained higher ultimate tensile strength and percentage elongation of 316L stainless steel.

15.5 Conclusions

The effect of welding process parameters: current, speed and gas flow rate on ultimate tensile strength and percentage elongation in TIG welding of AISI 316L stainless steel materials have been studied. The following points can be concluded from the experiments and analyses:

1. Response surface methodology (RSM) is found to be very helpful in the process of optimization carried out in the present study. Here the predicted value obtained from the models is very near to the experimental value.
2. Gas flow rate is the most important welding parameter which affecting the ultimate tensile strength, and it is followed by welding current and welding speed.
3. The most significant factor affecting percentage elongation is welding current and the next important factor in this context is gas flow rate followed by welding speed.
4. Welding speed is not found to be most significant at all in affecting either UTS or percentage elongation.
5. It is observed that both UTS and percentage elongation increase with increasing in the levels of welding process parameters up to its centre value; thereafter, the responses start decreasing with increasing in the levels of process parameters.
6. An optimum tensile strength of 643.83 MPa and percentage elongation of 14.68 are obtained under the welding conditions of current at 129.8 A, speed at 15.2 cm/min and gas flow rate at 8.7 l/min.
7. The error between predicted and confirmatory test is obtained approximately 1%, which validates the used optimization technique.

Acknowledgements The authors would like to acknowledge Dr. D. Bose, ME Department, NITTTR, Kolkata, West Bengal, for providing welding set-up for experiment for the present research work.

References

1. Ghosh, N., Pal, P.K., Nandi, G., Rudrapati, R.: Parametric optimization of gas metal arc welding process by PCA based Taguchi method on austenitic stainless steel AISI 316L. *Mater. Today Proc.* **5**, 1620–1625 (2018)
2. Tarnq, Y.S., Yang, W.H.: Optimisation of the weld bead geometry in gas tungsten arc welding by the Taguchi method. *Int. J. Adv. Manufact. Technol.* **14**, 549–554 (1998)
3. Benyounis, K.Y., Olabi, A.G.: Optimization of different welding processes using statistical and numerical approaches—a reference guide. *Adv. Eng. Softw.* **39**, 483–496 (2008)
4. Gunaraj, V., Murugan, N.: Application of response surface methodology for predicting weld bead quality in submerged arc welding of pipes. *J. Mater. Process. Technol.* **88**(1–3), 266–275 (1999)
5. Kumar, A., Sundarajan, S.: Optimization of pulsed TIG welding process parameters on mechanical properties of AA 5456 aluminum alloy weldments. *Mater. Des.* **30**, 1288–1297 (2009)
6. Murugan, N., Parmer, R.S.: Effects of MIG process parameters on the geometry of the bead in the automatic surfacing of stainless steel. *J. Mater. Process. Technol.* **41**(4), 381–398 (1994)
7. Benyounis, K.Y., Olabi, A.G., Hashmi, M.S.J.: Optimizing the laser-welded butt joints of medium carbon steel using RSM. *J. Mater. Process. Technol.* **164–165**, 986–989 (2005)
8. Zhao, Y., Zhang, Y., Hu, W., Lai, X.: optimization of laser welding thin-gage galvanized steel via response surface methodology. *Opt. Lasers Eng.* **50**, 1267–1273 (2012)

9. Olabi, A.G., Alsinani, F.O., Alabdulkarim, A.A., Ruggiero, A., Tricarico, L., Benyounis, K. Y.: Optimizing the CO₂ laser welding process for dissimilar materials. *Opt. Lasers Eng.* **51**, 832–839 (2013)
10. Ahn, J., Chen, L., Davies, C.M., Dear, J.P.: Parametric optimisation and microstructural analysis on high power Yb-fibre laser welding of Ti-6Al-4V. *Opt. Lasers Eng.* **86**, 156–171 (2016)
11. Ragavendran, M., Chandrasekhar, N., Ravikumar, R., Saxena, R., Vasudevan, M., Bhaduri, A.K.: Optimization of hybrid laser-TIG welding of 316LN steel using response surface methodology (RSM). *Opt. Lasers Eng.* **94**, 27–36 (2017)
12. Padmanaban, G., Balasubramanian, V.: optimization of laser beam welding process parameters to attain Maximum tensile strength in AZ31B magnesium alloy. *Opt. Laser Technol.* **42**, 1253–1260 (2010)
13. Elatharasan, G., Senthil Kumar, V.S.: An experimental analysis and optimization of process parameter on friction stir welding of AA 6061-T6 aluminum alloy using RSM. *Procedia Engineering* **64**, 1227–1234 (2013)
14. Srivastava, S., Garg, R.K.: Process parameter optimization of gas metal arc welding on IS:2062 mild steel using response surface methodology. *J. Manufact. Process.* **25**, 296–305 (2017)
15. Lakshminarayanan, A.K., Shanmugam, K., Balasubramanian, V.: Effect of autogenous arc welding processes on tensile and impact properties of ferritic stainless steel joints. *J. Iron Steel Res. Int.* **16**(1), 62–68 (2009)
16. Kumar, N., Mukherjee, M., Bandyopadhyay, A.: Study on laser welding of austenitic stainless steel by varying incident angle of pulsed laser beam. *Opt. Laser Technol.* **94**, 296–309 (2017)
17. Ghosh, N., Pal, P.K., Nandi, G.: Parametric optimization of MIG welding on 316L austenitic stainless steel by Grey-Based Taguchi method. *Procedia Technol.* **25**, 1038–1048 (2016)
18. Ghosh, N., Rudrapati, R., Pal, P.K., Goutam, N.: Parametric optimization of gas metal arc welding process by using Taguchi method on ferritic stainless steel AISI 409. *Mater. Today Proc.* **4**, 2213–2221 (2017)